FINITE ELEMENT ANALYSIS OF IMPLANTED PROXIMAL TIBIA

Name of Student and ID:

HAOQIAN QIAN 2187151

Academic Qualification:

Master of Biomedical Engineering

Principal Supervisor:

Professor Mark Taylor

Date of Report Submitted:

Monday, 27 May 2019

Submitted to the College of Science and Engineering in partial fulfilment of the requirements for the degree of Master of Engineering (Biomedical) at Flinders University, Adelaide, Australia

DISCLAIMER

I certify that this work does not incorporate without acknowledgment any material previously submitted for a degree or diploma in any university; and that to the best of my knowledge and belief it does not contain any material previously published or written by another person except where due reference is made in the text.

HAOQIAN QIAN

May 2019

ACKNOWLEDGEMENT

I would like to express my sincere appreciation to my supervisor Mark Taylor for his assistance. My special thanks are also extended to research fellows: Maged Awadalla, Dermot O'Rourke and Rami M. A. Al-Dirini for their valuable guidance through the computational modelling method.

ABSTRACT

Despite the poor initial stability of the cementless fixation, the osteointegration of an uncemented knee replacement is still the ultimate destination of a desired total knee replacement solution for knee osteoarthritis (OA) at the moment. To achieve bone ingrowth onto the implants, micromotion has been an inevitable parameter to interrogate in the study of knee implant primary stability. Considering that the complexity of the contact issues, coupled with uncemented fixation, could result in different magnitude of micromotion or micromotion patterns, we can have a hypothesis that such surface morphological parameters as flatness is likely to have an effect on micromotion. Therefore, the aim of this thesis is to incorporate the uneven surgical tibial cut into the finite element models and try to find out the effect of flatness of the surgical cut on micromotion at the tibial-bone interface. This study generates finite element models from nine surgical resected proximal tibiae and a commercial available tibial tray design from DePuy, and simulates loadings from level gait to examine the effect of flatness on the micromotion between the implant and the bone. What is found is that the flatness of the resected proximal tibia is moderately correlated with the peak micromotion at the interface during level gait. Moreover, the peak micromotion occurs at minimal ML loads, moderate axial loads, AP loads and FE moment but maximal IE moment and minimal VV moment in one cycle. Finally, loadings have a more dominant effect on when the micromotion occurs, while surface morphology is likely to have a more dominant effect on where the micromotion occurs and its corresponding magnitude in an uneven surface. This brings flatness as a variable to consider into the finite element model and the needs to also explore more activities, implant designs, cycles, sample groups to further investigate the relationship between the flatness of the surgically resected surface and the micromotion at the interface of the implant and the bone.

TABLE OF CONTENTS

LIST OF FIGURES

LIST OF TABLES

ABBREVIATIONS AND SYMBOLS

A	anterior
L	lateral
M	medial
P	posterior
AP	anterior-posterior
SI	superior-inferior
ML	medial-lateral
FE	flexion-extension
IE	internal-external
VV	varus-valgus
CT	computed tomography
OA	osteoarthritis
UHMWPE	ultra-high-molecular-weight polyethylene
HU	the Hounsfield unit
CT#	computed tomography number
ρ	apparent density (g/cm^3)
E	Young's modulus (MPa)
ν	Poisson's ratio
U	displacement (mm)
RMSE	root mean square error (mm) in this thesis mainly represents flatness
CPM	composite peak micromotion
AC	anterior-central
HA	hydroxyapatite
MBT	Mobile Bearing Tibial
LCS	Low Contact Stress
FEA	Finite Element Analysis

INTRODUCTION

With the increase of obesity, life expectancy as well as the decrease in mortality rate, non-fatal diseases like osteoarthritis have become a global burden, affecting approximately 303 million people in the world (accounting for almost 4% of the world population). Knee osteoarthritis (OA) alone affects around 263 million people worldwide (3.46% of the population) with a climbing incidence each year (GBD 2017 Disease and Injury Incidence and Prevalence Collaborators 2018, pp. 1789-858). According to the National Health Survey (NHS) 2014-2015 (Australian Bureau of Statistics 2015), 2.06 million people (about 8.7% of the Australian population) suffer from OA, which accounts for about 59% of all arthritic diseases in 2014-2015. Osteoarthritis, as the most common arthritis, is a joint disease with the joint cartilage breakdown as well as the underlying bone (National Institute of Arthritis and Musculoskeletal and Skin Diseases 2016).

There is no cure for OA at the moment, therefore joint replacement has been one of the most effective ways to treat end-stage OA, however, the lifespan and the performance of prosthesis could be worrisome sometimes (Glyn-Jones et al. 2015, pp. 376–87). In terms of cementless fixation, there are two leading causes of revision surgery in total knee replacement for patients over 80 years old, which are loosening (23.7%) and infection (21.4%) (AOANJRR 2018), indicating that implant stability is of vital significance to the revision rate. Cemented fixation accounts for more percentage of the joint replacement statistically thanks to its better initial fixation, however, cemented implants tend to fail in younger and more active patients. Therefore, uncemented fixation is potentially a better alternative for them since it allows the implant to form a more stable and durable bonding with the bone. According to the Australian Orthopaedic Association National Joint Replacement Registry (AOANJRR 2018), in the first of six months after the procedure, uncemented prosthesis often has a higher revision rate due to its weak initial bonding with the bone, nevertheless has a lower revision rate after a year of operation. There have been case studies that have shown similar performance between the cemented implant and cementless implant (Baker et al. 2007, pp. 1608-14). However, in general, registry studies have reported higher revision rates for cementless implants but in more active and younger patients (AOANJRR 2018).

Unlike the cemented fixation in knee replacement, where the mechanical loading is borne with the cement lying between the bone and the prosthesis, cementless fixation has a different

loading regime. It is because of the direct contact of the proximal tibia with the tibial tray, the contact problem becomes an important factor during cyclic loadings. However, since the complexity of contact analysis in the finite element model, the unevenness of the resected surface of the proximal tibia has not been investigated so far especially in silico studies. All previous studies regarding cementless fixation tibial tray assume that at the bone and the prosthesis interface, there is a perfectly clean-cut, which assumes that the surgical cut is flat, and this hypothesis lacks some considerations. One of the most significant advantages of cementless fixation over cemented fixation is osteointegration. However, excessive micromotion can lead to failure of osteointegration and ultimately causing implant loosening, failure, and revision. Therefore, it becomes somehow crucial to understand the effect of flatness on micromotion in a cementless knee replacement, especially at the interface of the tibial tray and the proximal tibia. In the hope of optimizing the finite element model and expanding our current understanding of the biomechanics relationships in the knee joint, it is also essential to incorporate these variables into the model.

LITERATURE REVIEW

Knee Joint Structure

Anatomy

Knee, as the largest and most complex joint in the human body (Kulowski 1932 pp. 618–63), is composed of both hard tissues like bones and soft tissues like cartilage, ligaments, and tendons. As illustrated in Figure 1, three major bones are connecting the knee joint including the distal end of the femur, the proximal end of tibia, the proximal end of the fibula and the patella (Gill et al. 2009, pp. 2377-85). And there are two major joints involved in this structure: the tibiofemoral joint and the patellofemoral joints. The knee joint is mainly referred to as the tibiofemoral joint, which is the joint where the proximal tibia and the distal femur met in this thesis. To be specific, the tibiofemoral joint normally has two articulation centers. One is the lateral region of the femoral condyle with that of the tibial plateau, while the other one is the medial region of the femoral condyle with that of the tibial plateau (wikipedia 2019).

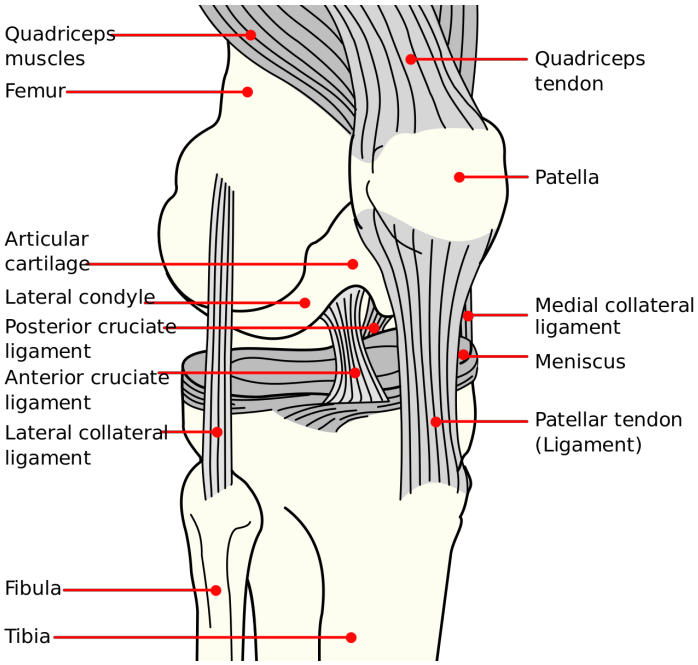

Figure 1: Anatomy of the knee joint

(wikipedia 2019)

Cartilage

Articular cartilage is located at the end of tibia and femur as well as at the back of the patella to protect bones from excessive friction while sliding over each other during the articulation with the help of synovial fluid and bursa (sacs filled with fluid). It is also able to withstand tension as well as shear stress during loadings to protect the underlying proximal tibia or distal femur (Costi 2017). One of the most common knee OA is due to the wear of the hyaline cartilage at the ends of the bones and since its metabolism is much slower than bone, it is almost impossible to regenerate them via exercise or self-restoration.

As a type of fibrous cartilage, meniscus functions to withstand pressure and take the load. Like the annulus fibrosus in the intervertebral disc of the human spine, it acts as a shock absorber (Costi 2017). With the shape of a crescent, lateral menisci and medial menisci sit on top of the corresponding condyle of the tibial plateau respectively (Platzer 2004, p. 208). The concave shape of meniscus also allows the convex shape of the femoral condyle to have congruence during contact. Additionally, as another type of cartilage, it also lubricates the knee joints and reduces friction during rotational moments (Costi 2017).

Ligaments

Ligaments are crucial in maintaining the stability of the knee joints and limiting ranges of motion of the knee joint during all types of activities. For instance, anterior cruciate ligaments (ACL), posterior cruciate ligaments (PCL), medial collateral ligaments (MCL) and lateral collateral ligaments (LCL) all play a vital role in keeping the femur and the tibia in place in rotations like knee bending or twisting as well as translation or sliding (Costi 2017). Without them, the range of motion can easily exceed its standard value, ending up with a floppy knee.

Muscles

Muscle is connected to the bones by tendons and it plays an important role in generating forces and realizing skeletal movement actively. The main muscles around the knee joints are quadriceps muscles (mainly responsible for extension of the knee joint), hamstrings muscles and gastrocnemius muscles which are closely related to the forces acting on the knee joint.

Knee Biomechanics

Range of Motion

As the largest joint in the human body (Kulowski 1932, pp. 618-63), the knee has 6 degrees of freedom (DOF) including three translations: anterior-posterior (AP), superior-inferior (SI), medial-lateral (ML) and three rotations: flexion-extension (FE), internal-external (IE), varus-valgus (VV). It has a more complex degrees of freedom than a simple hinge joint which only has one degree of rotational freedom, where the flexion-extension rotation ranges from - 5° up to 160°, the VV rotation ranges from 6° to 8°, the internal-external rotation ranges from 25° to 30°, the anterior-posterior translation ranges from 5 mm to 10 mm, the SI translation ranges from 2 mm to 5 mm and the medial-lateral translation ranges from 1 mm to 2 mm (Masouros et al. 2010, pp. 84-91). In reality, the biomechanics of the knee joint is coupled with rolling, sliding, and rotation between the femur and tibia.

Forces

Joint contact forces estimated indirectly by calculating from external forces (like recorded ground reaction forces), muscles forces, as well as geometric measurement, can trace back to 1960s thanks to the introduction of motion analysis. However, this technique is often coupled with inaccuracy with the assumptions like the line of action or unbalanced activities of the relative muscles (Nissan 1980, pp. 375-81). Conversely, the direct measurement using telemetry direct from the implants can give us a more valid value. In knee arthroplasty engineering design, it is crucial to have a more trustworthy magnitude of forces and moments in various types of activities acting on the implants to be able to determine the suitable material and its geometry and other factors to secure the prosthesis is safe and sustainable.

The forces acting on the tibial tray could give rise to the full range of motion as described above. To simplify the loads into a representative finite element model. The loads can be applied to four regions laterally, medially, posteriorly and anteriorly. The direction of the forces could fall into three categories: AP direction, ML direction, and axial direction. The anterior and posterior axial forces potentially generate SI translation as well as the FE moment. The medial and lateral axial forces can produce SI translation as well and VV moment. The AP direction forces acted on the medial and lateral region of the tibia can cause

AP translation as well as IE moment. The ML direction forces acted on the medial and lateral region of the tibia can cause ML translation only.

Knee Arthroplasty

The knee replacement has been around for approximately 50 years and the goal is to reduce pain, restore the basic functions of the remaining life of the patient (Palmer & Cross n.d.). However, with the complexity of the six degrees of freedom of the knee joint, it is difficult to have an as optimistic outcome as the hip replacement. Compared with the ball-socket model of the hip, the modified ball on plate model needs to be able to realize a more complicated range of motion by using only a few main components.

The current total knee replacement can be divided into four major components: femoral component, tibial tray, tibial bearing component and patella component (Mow & Huiskes 2004, p. 657). As illustrated in below Figure 2, most femoral and tibial components are made from cobalt-chrome alloy or titanium alloy while the bearing surface in between is usually made of ultrahigh-molecular-weight polyethylene (UHMWPE), representing meniscus which allows two metal component to rotate or slide with lower friction. This thesis mainly focuses the tibial component.

Image has been removed due to
copyright restriction.

Figure 2: LCS Complete (Sorrells 2014)

Cementless Fixation

Cemented fixation has the maximum fixation at the start, but it has a higher revision rate in younger and more active patients due to the asymmetric loading (Matthews & Goldstein 1986, pp. 27-33). In comparison, cementless fixation is more suitable for younger and more active patients and thus has a much challenging loading regime than cemented one. There are major four various types of cementless fixation including the simple press-fit, porous-coated,

hydroxyapatite (HA) coated and hybrid (with both porous and HA-coated). In simple press-fit fixation, the diameter of the implant is typically slightly bigger than the resected diameter of the keel so that when the surgeons implant the prosthesis, they will hammer down the implant into the prepared bone, allowing the interface to have a mechanical lock. The porous-coated implants, on the other hand, promotes bone ingrowth onto them and adds extra grip at the interface. HA-coated implants apply materials hydroxyapatite, which is a very similar material to our natural bone mineral, to enhance bone ingrowth as well. All these fixation methods are designed to achieve trabecular bone ingrowth onto the implant. What's more, since there is no cement between bone and implant, there will be free of bone-cement debris as well as implant-cement debris. Finally, the study (Chong et al. 2011, pp. 948-54) has shown that cementless fixation helps to preserve the tibial bone stock and maintain postoperative stability.

According to the Australian Orthopaedic Association National Joint Replacement Registry (AOANJRR 2018) found that uncemented prosthesis has a higher revision rate during the initial stage after the surgery but a lower revision rate after a year of operation. In a radiograph follow-ups, Aebli and fellows (Aebli et al 2004, pp.783-9), as demonstrated in below Figure 3 have found that after operation, a higher density of radiolucent line and a larger gap between the implant and bone is seen on the radiograph at the implant-bone interface with only the middle keel is exempted. After two years of operation, the radiolucent lines disappear and the gap has been narrowed. After eight years of operation, the implant and the bone almost osteointegrated without an apparent sign of radiolucency. The presence of radiolucent lines in the radiograph could indicate the appearance of fibrous tissues generated from the relative motion of the implant and the bone.

Image has been removed due to
copyright restriction.

Figure 3: Radiographs of implanted cementless tibial tray of same knee
(A) Postoperatively (B) Two years postoperatively (C) Eight years postoperatively (Aebli et al. 2004, pp.783-9)

Although cementless fixation has lots of advantages over cemented one, it also coupled with a few problems. Critical study (Lombardi, Berasi & Berend 2007, pp. 25-9) revealed several clinical evidence including poor fixation proven by the occurrence of radiolucent lines, osteolysis, aseptic loosening, and dislocation. To be able to realise bone ingrowth, micromotion between bone and implant need to be less than 50 μm and if it is over 150 μm (Pilliar, Lee & Maniatopoulos 1986, pp. 108-13), a non-mineralized fibrous tissue can form at the interface, causing failure of bone ingrowth onto the implant and thus considerably affecting implant stability.

Surgical Cut

In the knee replacement procedure, surgeons resect the proximal tibial part according to the surgical instructions from the manufacturer with a thin oscillating saw via a slot. And as a result, a clinical surgical cut is often uneven, which could be an important variable to consider while studying stress or strain. Early studies have found an average roughness of 1.71 mm (ranging from 1.06 to 2.57 mm) and flatness of 0.26 mm (ranging from 0.16 to 0.38 mm) of surgical proximal tibial cut (Toksvig-Larsen & Ryd 1991, pp. 15-8; 1994, pp. 63-6). Taylor,

Tanner and Freeman (1998, pp. 303-10) also found that surface morphology has a large effect on the stress of the cancellous bone in a cementless prosthesis. And studies have also shown that gap exceeding 0.3-0.5 mm could potentially prevent bone ingrowth (Sandbom et al. 1987, p. 217; Carlsson et al. 1988, pp. 272-5). However, no significant studies have correlated surface morphology with micromotion in uncemented fixation so far. Therefore, this thesis aims to study the effect of variation of flatness of the surgical tibial cut on the micromotion at the tibial tray-bone interface.

Previous Cementless Studies

Over the last 30 years, studies of various cementless tibial components have been performed with an ultimate focus on micromotion as depicted in Table 1. Previous in vitro study compared five various tibial tray designs under different loadings including vertical, anterior-posterior shear and internal-external rotation (Walker, Hsu & Zimmerman 1990, pp. 245-53). Keja and fellows (1994, pp. 275-83) used different fixation methods with an axial load to a flat metal surface to generate a micromotion map across the tibia using finite element modeling. Tissakht, Eskandari and Ahmed (1995, pp. 365-75) applied a vertical compressive load to four different cadaveric tibiae to validate the computational model, resulting in different relative displacement due to different fixations. Kraemer, Harrington and Hearn (1995, pp. 227-235) applied eccentric axial, torsional and shear cyclic loads to four different tibial trays on nine pairs of tibiae using a linear variable differential transformer (LVDT) to find out the effect of different fixation methods of the tibial tray. Hashemi, Shirazi-Adl and Dammak (1996, pp. 257-67) applied normal and tangential loads to the interface of a beaded porous-coated metal plate and the cancellous bone cube prepared from various regions of four resurfaced cadaveric tibiae to correlate tangential displacement and friction parameters.

In an in vitro study, Sala, Taylor and Tanner (1999, pp. 610-5) applied axial and cyclic torques to a tibial tray on nine pairs of healthy cadaveric tibiae to relate torsional micromotion and fixation methods. Relationships between implant migration and the post-operative biomechanical environment have been reported by Perillo-Marcone and fellows (2004, pp. 1205-13) in a finite element and radio stereometric analysis (RSA) study. A previous finite element study figured out the relationships between shear micromotion and degrees of flange curvature by applying an axial load to the medial or lateral condyle of the tibial plateau

(Barker, Tanner & Ryd 2005 pp. 449-56). Chong, Hansen and Amis (2010, pp. 1074-80) used in vitro and in silico methods to determine the relationships between different loading cases and peak micromotion/surface area. Taylor, Deffenbaugh and Heldreth (2010, Poster No. 2114) have reported micromotions of an entire gait cycle of six tibial tray orientations, making use of finite element and KneeSim analysis. A more comprehensive loading has been studied in different implant designs with in vivo data including level gait, stair ascent, stair descent, stand to sit and deep knee bend (Taylor, Barrett & Deffenbaugh 2012, pp. 1362-8). A large-scale finite element analysis has been performed by Galloway and fellows using 328 models and various types of loading like anterior-posterior, medial-lateral, axial forces as well as FE, VV, IE rotational moments (Galloway et al. 2013, pp. 1900-6). Fitzpatrick, Hemelaar and Taylor (2014, pp. 1718-26) used surrogate modeling to discover the variations of micromotion in 30 different gait cycles from six patients. The most recent study by Navacchia and fellows (2018, pp. 115-23) determined the micromotion in different activities, using synthetic bone and four tibial trays, by the means of digital correlation (DIC) and finite element modeling.

Authors	Method	Subjects	Loadings	Outcomes
Walker, Hsu & Zimmerman 1990	In-vitro	5 tray designs, artificial and cadaver bone	vertical central, vertical offset (VV), AP shear and IE torque	Implants design/ loading configurations vs interface micromotion
Keja et al. 1994	FEA	a flat metal tibial prosthetic surface	an axial load	micromotion across tibia vs fixation (perimeter, midcondylar)
Tissakht, Eskandari & Ahmed 1995	FEA & In-vitro	FEA model from 1 tibia, 4 cadaveric tibiae for in vitro	vertical compressive load	relative displacement vs fixation method vs friction coefficient
Kraemer, Harrington & Hearn 1995	In-vitro (LVDT)	4 tibial trays, 9 pairs of tibiae	eccentric axial (lateral, medial, posterior & anterior), torsional & shear cyclic loads	micromotion vs fixation (screws, pegs and keels)
Hashemi, Shirazi-Adl & Dammak 1996	In-vitro & FEA	bone cubes prepared from 4 resurfaced cadaveric tibiae	normal & tangential load	friction resistance vs relative tangential displacement
Taylor, Tanner & Freeman 1998	FEA, published migration & survivorship comparison	model from 1 tibia	uni- & bi-condylar load	surface morphology vs cancellous bone stress vs implant migration
Sala, Taylor & Tanner 1999	In-vitro	9 pairs of healthy cadaveric tibiaee, 1 tibial tray	axial loads & cyclic torque	torsional micromotion vs fixation

Authors	Method	Subjects	Loadings	Outcomes
Perillo-Marcone et al. 2004	FEA & RSA	1 cementless, 1 cementless & porous, 1 cemented, 1 cementless & HA	axial load to medial & lateral condyle	post-operative mechanical environment vs implant migration
Barker, Tanner & Ryd 2005	FEA	15 trays and 1 bone	axial load either to medial & lateral condyle or a unicondylar load	shear micromotion vs degrees of flange curvature
Chong, Hansen & Amis 2010	In-vitro & FEA	In-vitro: 8 cadaveric tibiae	vertical load with 70%/30% ML load share and AP/ML shear force, peak vertical load at 25% of the stair climbing cycle with AP shear at tibial-femoral contact points of specific knee flexion angle	peak micromotion/ surface area vs loading conditions
Taylor, Deffenbaugh & Heldreth 2010	FEA & KneeSim	model from 1 tibia, LCS and Duofix tibial trays	entire gait cycle, 6 tibial tray orientations	micromotion & strain
Taylor, Barrett & Deffenbaugh 2012	FEA	model from 1 tibia, PFC Sigma, LCS Complete Duofix & LCS Complete MBT	level gait, stair ascent, stair descent, stand to sit and deep knee bend from Orthoload	micromotion
Galloway et al. 2013	FEA	328 models	AP, ML & axial forces and FE, VV & IE rotations, time normalised from 0 to 100% gait	peak strain in the bone of the resected surface
Fitzpatrick, Hemelaar & Taylor 2014	Surrogate Modelling	model from 1 male, 30 gait cycle trials from 6 patients	6-DOF TF joint loads	micromotion vs gait cycle
Navacchia et al. 2018	In-vitro (DIC) & FEA	synthetic bone, 4 tibial trays, TKR model and tray-only model	gait, stair descent & deep knee bend	micromotion vs cycle/activities/ surface area/different models

Table 1: Outlines of previous studies regarding cementless tibial tray

Considering the significance of micromotion in uncemented fixation and the unevenness of the resected surgical cut described above, we can have a hypothesis that surface morphological parameter like flatness might and is highly likely to influence micromotion. As limited numbers of finite element studies have interrogated flatness into the simulation, this study will incorporate this factor into the model. Hence, this thesis aims to study the effect of flatness of the surgical tibial cut on the micromotion at the tibial tray-bone interface.

METHODOLOGY

Specimens

The models are generated from nine cadaveric left tibiae with resected surfaces, which has been prepared in vitro with Low Contact Stress (LCS) Complete Mobile Bearing Tibial (MBT) tray manufactured by DePuy Synthes Joint Reconstruction according to the corresponding surgical instructions. Therefore, unlike other cementless knee replacement finite element analysis, this study incorporates the uneven surface morphology of the surgical cut into the finite element model. To be able to turn these cadavers into digital information, all specimens are scanned in a clinical CT scanner with wraps or salines around them. Hence, the images that we obtained need to be segmented and calibrated in the post-processing steps.

Image Segmentation and Transformation

Segmentation

Segmentations of the tibiae are conducted using Simpleware™ ScanIP (Synopsys®, Inc., San Jose, US) with multi-slice CT images with a voxel size of 0.49x0.49x0.63 mm. For each resected tibial bone image, a stack of almost 600 transverse slices is reconstructed (up to about 370 mm in length), producing a total dataset of around 100MB. Pixels of the raw images without calibration have grey level values from - 1000 to 2000. It can computationally and visually select the bone area (region of interest: ROI) from the surrounding artifacts like wrappers or fluids via Simpleware. Threshold-based segmentation is used. An appropriate range of the Hounsfield unit or greyscale is chosen for each section of the tibia and subsequently, a mask is applied over the bone on each slice to separate the bone and the surroundings in the final 3D object.

In the middle shaft of the tibia the greyscale level is much higher since the cortical bone is thicker and denser, while in the proximal and distal ends of the tibia, the greyscale level is largely decreased due to the cortex thinning and these are the area where we need to spend more efforts in. It is important to adjust the greyscale threshold (a lower and upper boundary of the greyscale) in each region and then manually fill up the outline of the bone on each slice (as demonstrated in Figure 4). At the resected uneven surface of the proximal tibia, a 3D wrap tool is applied. The images are linearly interpolated every 10 slices to give a smoother

transition of the resected surface and to decrease unnecessary artifacts during computational simulations. At the resected area of the keel, another mask is applied and each slice is manually segmented and once finished, a Boolean operation is implemented to subtract the keel from the proximal tibia. Eventually, a Recursive Gaussian filter is applied to the mask to reduce the noise and smooth out the surface area.

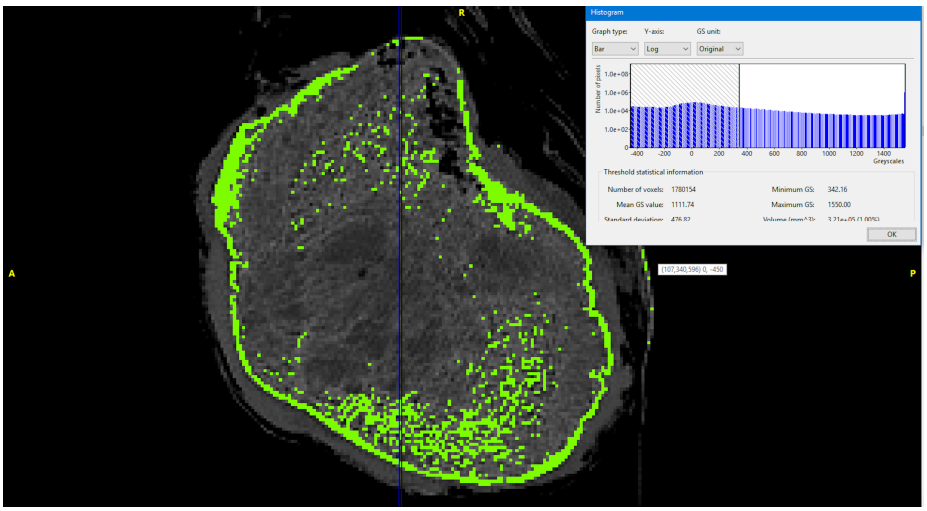

Figure 4: Image segmentation Greyscale threshold in proximal tibial trabecular

Transformation

To be able to match the material property from ScanIP to Hypermesh as well as the loading data, later on, all models need to be transformed into the global coordinate in ScanIP in advance. Two points (one vector) are selected manually at the resected surface on each plane (coronal plane, transverse plane, and sagittal plane respectively) to align with the global axis: x, y, and z respectively. As this step involves rotation, the alignment will create an empty image to suit the new position, therefore shrink wrap is used subsequently to crop the data and remove the space around the bone automatically (Synopsys, Inc. 2016). Finally, the segmented and transformed mask and the image are exported to a finite element surface model as an STL file to use later.

Material Properties

Tibial Tray

The LCS MBT is made of Titanium alloy (Ti6Al4V) and its mechanical properties are modeled with a density of 4.43 g/cm^3, Young's modulus of 115 GPa and Poisson's ratio of 0.3.

Bone

Thanks to the heterogeneous microarchitecture of the bone, a simple constant could not simply be assigned to the whole tibia. The most common way to interpret the digital image data into the valuable mechanical property of such non-homogenous material as the bone is first, to correlate Hounsfield unit of the multislice computed tomography images into density and then correlate bone density into the mechanical parameters like Young's modulus.

Greyscale ⇒ Bone Density (Linear)

The Hounsfield unit (HU), also called CT number (CT#), is closely associated with the attenuation coefficient of various mediums. It also has a large difference within such heterogeneous tissue as a bone. Apparent density (ρ, g/cm^3) is of linear relationship with the Hounsfield unit (HU). The two calibration points are selected in the bone marrow and the cortical bone respectively. Bone marrow is considered to have 0 apparent density, while the cortical bone apparent density is set to 1.73 g/cm^3 (Carter & Hayes 1997, pp. 954–62; Ghosh et al. 2015, pp. 697-710; Bryan et al. 2010, pp. 57-65; Awadalla et al. 2018, pp.1876-86).

Bone Density ⇒ Young's Modulus (Exponential)

A literature review (Helgason et al. 2008, pp. 135-46) has depicted the mathematical relationships between bone density and its corresponding mechanical properties. Among them, Morgan, Bayraktar and Keaveny (2003, pp. 897-904) had determined the power-law regression between Young's modulus (E, MPa) and an apparent density (ρ, g/cm^3):

$E = 10.00 + 6500.00 * \rho^{1.49}$.

After applying these two relations, a representative 3D model can be visualized via generating a finite element model as demonstrated in below Figure 5, material properties of each tetrahedra element can be generated, viewed and exported as INP file to use later.

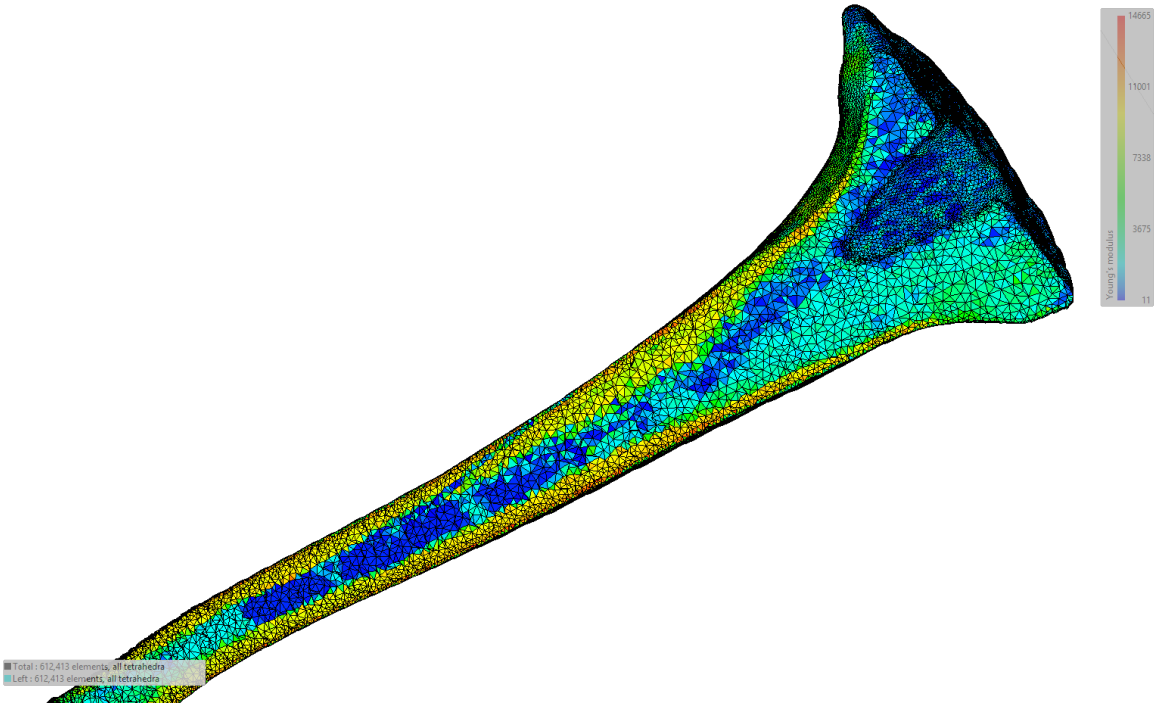

Figure 5: Young's modulus (MPa) of the resected tibia (3D representation)

Virtual Implantation and Meshing

All prostheses are manually implanted onto the resected proximal tibia via Hypermesh (Altair Engineering, Inc., Michigan, US). First, import the prosthesis X_T file from the manufacturer and rescale 100 and then import the STL file from the surface model of the tibia that is generated previously from Simpleware. Secondly, translations in x, y and z-direction are essential to finely align the prosthesis with the bone as demonstrated in Figure 6. Once the implant and the bone is aligned properly, shrink wrap is applied. A loose wrap is implemented here to avoid any sharp changes in the surface geometry. Subsequently, a finite element surface is generated from all the elements and then turned into a solid to realize any solid edit if required. Since this study will not investigate impaction, the Boolean operation is conducted to remove the implant from the tibia. However, to be able to study the influence of the unevenness on the micromotion, the Boolean operation does not subtract all the resected proximal surface, and as a result, only small regions undergo the Boolean operation, resulting most areas are still uneven. In this thesis, the more the bone is cut, the higher degree of Boolean operation is. Moreover, because the implant studied is for primary total knee replacement, only half the tibiae are simulated to save computational cost and time, Hence,

the distal part of the tibiae is trimmed off using solid edit as well. Eventually, referring to a recent study (Awadalla et al. 2018, pp.1876-86), a linear tetrahedral element with a size of 1 mm is used for volumetric meshing for both components and for all models with about 18,339 nodes and 78,469 elements for MBT and approximately 65270 nodes and 314565 elements for the resected half tibia. To be able to simulate the model in Abaqus later, all mesh files of entire bones, prosthesis as well as their corresponding faces are saved as INP file.

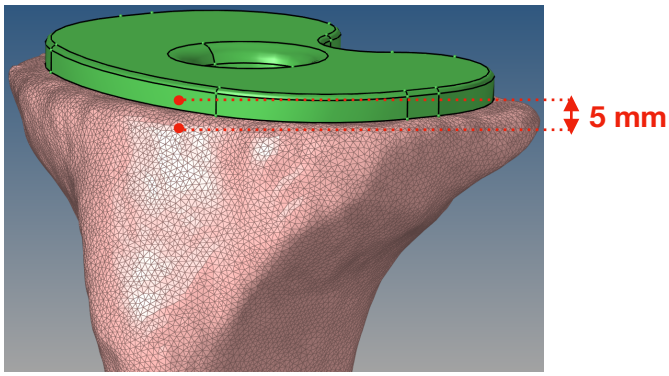

Figure 6: Virtual Implantation and AC paired nodes location

Simulations

Simulations are run with a processor of Intel® Core™ i7-3770 CPU @ 3.40 GHz, 16 GB RAM, OS Windows 10 Enterprise 64 bit. Each cycle takes up to 1 hour to run in Abaqus/CAE version 6.14-3 (Dassault Systèmes Simulia Corp., Providence, RI, US) and another hour is required to calculate the displacement and micromotions and save the corresponding frames, coordinates, distances, peak micromotions, etc in Matlab (The MathWorks, Inc., Natick, MA, US). Multicycle loadings could take up to 3-4 hours to run for each session. The minimum time increment of the simulation has been set up to 10-6, where the number of equilibrium iteration needs to be bigger than the input threshold, otherwise, the model will have co penetration errors.

Boundary Conditions

Proximal End

Joint contact forces applied in this study are from Denver University, only covering parts of level gait: stance phase, heel strike and heels off (Fitzpatrick et al 2014, pp. 360-9).

At the proximal tibia, the loading file during level gait is applied to the finite element model. Level gait loadings are used instead of stair descent, stair ascent or deep knee bend is because

the previous study has shown that walking induces more percentages of peak micromotion than other activities of daily living (Taylor, Barrett & Deffenbaugh 2012, pp. 1362-8). The loads consist of three moments: FE, IE, and VV as well as three translation: SI, ML, and AP, as demonstrated in below Figure 7, Figure 8 and Table 2:

Directions\Regions	Anterior	Posterior	Lateral	Medial
Axial	✓	✓	✓	✓
Medial-Lateral	✗	✗	✓	✓
Anterior-Posterior	✗	✗	✓	✓

Table 2: Loading file to the proximal tibia tray

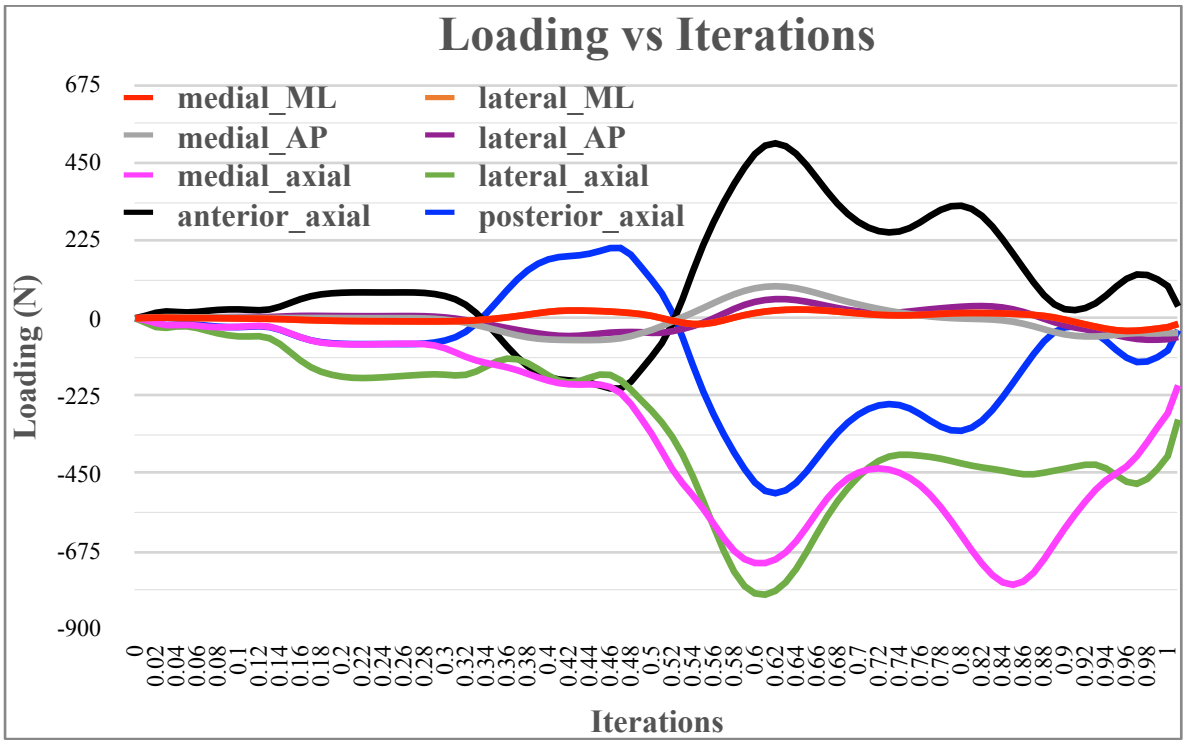

Figure 7: Forces vs iterations of one cycle during gait

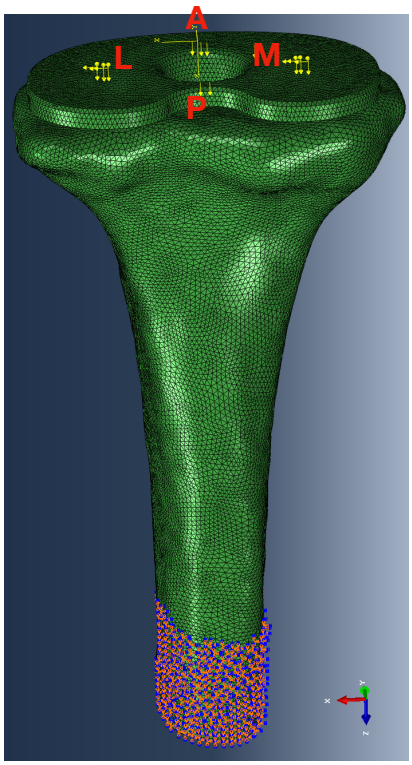

Figure 8: Boundary conditions of the proximal tibial model

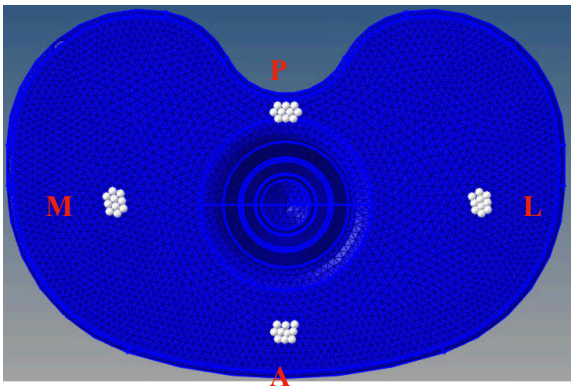

Figure 9: Node set where forces are applied to

Overall, the axial forces will contribute to SI translation but with different directions. A positive force as shown in above Figure 7 represents tension while a negative one represents compression. The axial forces anteriorly and posteriorly specifically (as shown in black and blue in above Figure 7) will contribute to the FE moment because they are always of opposite directions but the same magnitude. On the other hand, the axial forces laterally and medially will contribute to the VV moment since they have different magnitudes even though they are both compressive forces (as shown in green and pink in above Figure 7).

The medial-lateral force acting medially and laterally (as shown in red and orange in above Figure 7) will contribute to ML translation, while the anterior-posterior force acting medially and laterally will not only contribute to AP translation but also to IE rotation (axial rotation) because the medial AP force does not equal to the lateral AP forces (as highlighted in grey and purple solid line in above Figure 7).

Forces applied to the medial and lateral regions of the tray are distributed into 10 node sets for each region at an equal distance from the tray center as demonstrated in above Figure 9. Same for the forces applied to the anterior and posterior region of the tray. And all the forces applied to the tibial tray can represent the six degrees of freedom of the knee joint. Each loading cycle is discretized into 0.02 intervals and 51 increments. Due to the limited time of the study, only one cycle is simulated here.

Bone-Prosthesis Interface

The bone and implant interface is modeled as deboned and the friction of coefficient at the implant-bone interface is assumed to be 0.6 (Taylor, Barrett & Deffenbaugh 2012, pp. 1362-8). Small sliding and 0.2 degrees of smoothing for the master surface is allowed in the node to surface contact configuration, meaning that the master surface normals at the edge of the faces will be recalculated to avoid slave nodes being snagged on sharp corners while traveling along the master surface (Dassault Systèmes 2010). A 0.002 tolerance for slave adjustment is set up also, which means that during the contact, slave nodes that penetrate through the master surface or over closed are allowed to move 0.002 mm to enable the surfaces to converge. These will slightly change the surface flatness of the resected surface, but since the tolerance we set up is very small, the influence on the result is negligible (Dassault Systèmes 2010).

Distal End

The distal end of the tibia is constrained without relative translation or rotation. A custom Matlab code is used to find all distal node sets, by selecting the region from the minimal coordinate in the z-axis of the tibia (SI direction) to the 1/6 of the total length of the distal half tibia, as demonstrated in pink nodes in above Figure 8.

Micromotion

A custom Matlab code is used to find the closest nodes from the bone to the prosthesis and the two nodes that are recognized as the closest are referred to the paired nodes.

As an output of the simulation, displacement is the most important physical parameter we need to have to be able to calculate micromotion, formulas as below is implemented to calculate the micromotion:

$$U_1 = [(U_{1_c} - U_{1'_c}) - (U_{1_p} - U_{1'_p})] * 1000$$

$$U_2 = [(U_{2_c} - U_{2'_c}) - (U_{2_p} - U_{2'_p})] * 1000$$

$$U_3 = [(U_{3_c} - U_{3'_c}) - (U_{3_p} - U_{3'_p})] * 1000$$

$Micromotion(\mu m) = \sqrt{U_1^2 + U_2^2 + U_3^2}$, where

U_{1c} represents the displacement of the node on tibial tray in ML direction in the current frame

$U_{1'c}$ represents the displacement of the node on tibia in ML direction in the current frame

U_{1p} represents the displacement of the node on tibial tray in ML direction in the previous frame

$U_{1'p}$ represents the displacement of the node on tibia in ML direction in the previous frame

U_{2c} represents the displacement of the node on tibial tray in AP direction in the current frame

$U_{2'c}$ represents the displacement of the node on tibia in AP direction in the current frame

U_{2p} represents the displacement of the node on tibial tray in AP direction in the previous frame

$U_{2'p}$ represents the displacement of the node on tibia in AP direction in the previous frame

U_{3c} represents the displacement of the node on tibial tray in SI direction in the current frame

$U_{3'c}$ represents the displacement of the node on tibia in SI direction in the current frame

U_{3p} represents the displacement of the node on tibial tray in SI direction in the previous frame

$U_{3'p}$ represents the displacement of the node on tibia in SI direction in the previous frame

Subsequently, the Matlab code finds the peak micromotion during the entire cycle at these paired nodes and saves both the magnitude of the micromotion as well as the ID and coordinate of the paired nodes accordingly.

Another custom Matlab code is then run to generate the composite peak micromotion (CPM) map across the tibial tray, the interface distance between the bone and the prosthesis and the height deviation of the bone using above saved data. CPM map across the tibial tray is plotted

by finding the peak micromotion frame, the corresponding coordinates of the paired nodes in that frame as well as the magnitude of the micromotion calculated computationally in that frame for all paired nodes across the entire tibial tray. But this magnitude does not imply the direction of the micromotion or where the tray or bones move. The height deviation of the bone is plotted by selecting the regions from the maximum coordinate in the z-axis to a manually tolerated z coordinate beneath the maximum z vertices at the resected surface. One of the important things is to get the nodes as close as to the maximum z vertices but to be able to still visualize the entire resected proximal tibial surface simultaneously. The interface distance between the bone and the prosthesis is plotted by finding the coordinate of the paired node sets and its corresponding distance from each other which is generated using the previous step. To be able to visualize the variations of micromotion during the cycle. The finite element model is imported into Abaqus via a previously generated ODB file after simulation and unique nodes at the surface area of both bone and the prosthesis are manually selected respectively to generate the output field of displacement and saved as excel. And then using the identical micromotion calculation formulas as stated above, a 2D curve plot of micromotion versus iterations is obtained. Unlike the micromotion pattern plotted via Matlab, this 2D curve not only depicts the magnitude of the micromotion but also the relative motion in all three directions: U1: ML direction, U2: AP direction and U3: SI direction. And the value of U3, for example, indicates where the tray and bone relatively move. If U3 is a positive value, it means that the tray and the bone are moving away from each other and if U3 is a negative value, it means that the tray and the bone are moving towards each other.

Evaluation of Flatness

Deviation of the surface points from a reference plane defines flatness as demonstrated in Figure 10 (The International Organization for Standardization 2011, ISO 12781-1). According to ISO 12781-1 2011, there are two ways of defining a reference plane: the minimum zone reference plane, which is the arithmetic mean plane of two parallel planes that enclose the surface with the least separation and the least-squares reference plane, which is the plane that the sum of the squares of local flatness deviation is the minimum.

The flatness value can be quantified via root-mean-square flatness deviation ΔF_{rms}, which is the sum of the squares of the local flatness deviation from the least-squares reference plane.

Image has been removed due to
copyright restriction.

Figure 10: Local deviation relative to reference plane
(The International Organization for Standardization 2011, ISO 12781-1)

A custom Matlab code is used to quantify the flatness of the resected surface once the surface model that is contained in an STL file is generated in the previous step in Simpleware. First, all nodes need to be plotted from the STL file using three vertices from the matrix. Secondly, top nodes are identified and highlighted by finding the regions between the maximum coordinate in the z-direction (SI direction) and a manually adjusted tolerance z coordinate from the maximum vertices as demonstrated in Figure 11. The criteria to optimize this tolerant level is to get the z coordinate as closely as possible to the maximum z coordinate, but at the same time being able to select all the resected surface nodes. This could be realized by viewing the 3D plot in a transverse plane and see if the highlighted nodes form a continuous resected proximal tibial shape. Moreover, the linear polynomial surface fit function in Matlab is used to best fit all the previously selected surface nodes to a reference plane. Lastly, to be able to eventually quantify the flatness of the resected surface, the goodness of fit output is also used in the surface fit function to computationally calculate RMSE, which is used here to simplified the calculation of standard deviation to the reference plane introduced earlier.

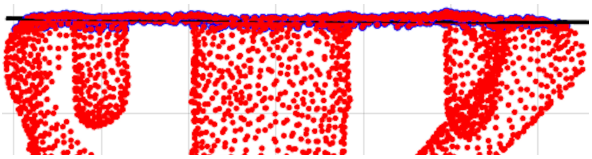

Figure 11: Reference plane of top surface nodes

RESULTS

Flatness

As specified in the methodology part, the flatness quantified via Matlab can be concluded as Table 3:

No.	Sample	RMSE (mm)
1	GL1605436L	0.36
2	GL1705910L	0.17
3	GL1706427L	0.41
4	GL1706555L	0.34
5	GL1707059L	0.02
6	GL1707254L	0.29
7	GL1707427L	0.27
8	GL1807511L	0.31
9	GL1807517L	0.43
MEAN		**0.29**
STANDARD DIVATION		**0.13**

Table 3: Root Mean Square Error (RMSE) of the top surface

The average flatness of nine left tibiae is 0.29 mm with a 0.13 mm standard deviation (ranging from 0.17 mm to 0.43 mm).

Micromotions Variation with Iterations

As specified in the methodology part, the relationships between iterations and micromotion that has been quantified via Abaqus can be visualized as below Figure 12, representing the micromotion variation of specimen GL1707254L of the entire cycle and the nodes selected to calculate the micromotion is respectively located at the anterior central edge of the tibial tray and vertically 5 mm underneath the contact interface on the outer surface of tibia as highlighted in red in above Figure 6. However, since the formula used to calculate the micromotion will always result in a positive value, the actual direction of the relative motion can be determined by U1 (micromotion in ML direction), U2 (micromotion in AP direction)

or U3 (micromotion in SI direction) respectively. For instance, as demonstrated in Figure 12, U3 represents the micromotion in the SI direction and the value is negative, meaning that the tibial tray and the underlying proximal tibia are moving towards each other in the SI direction. From the plot, we can also notice that the value of the relative motions of the tibial tray and the proximal tibia in the SI direction is sometimes positive and sometimes negative, which means that the bone and the prosthesis is moving towards each other sometimes and moving away from each other sometimes.

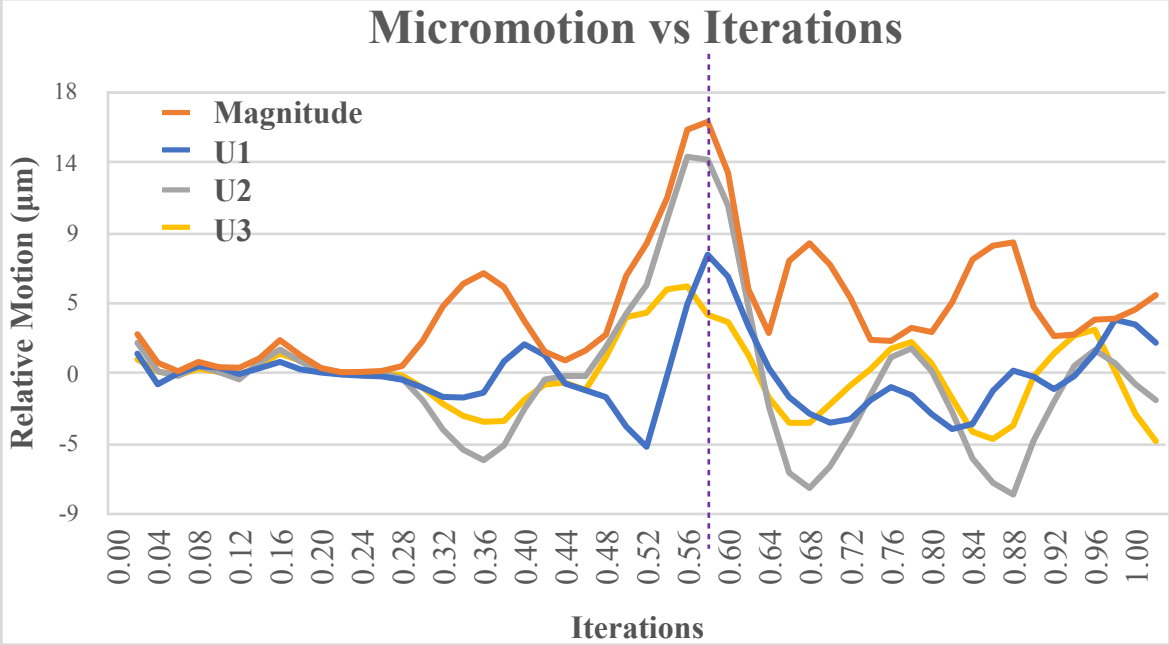

Figure 12: Micromotion vs iterations during gait of GL1707254L

It can also be easily seen that for all the nine left tibiae, the peak micromotion occurs during iterations from 0.56 to 0.58, where the vertical purple dash line as demonstrated in below Figure 13. The nodes selected to calculate the micromotions for all specimens are the same as above, which is at the AC edge of the tibial tray as well as vertically 5 mm underneath the contact surface of the bone and the tray.

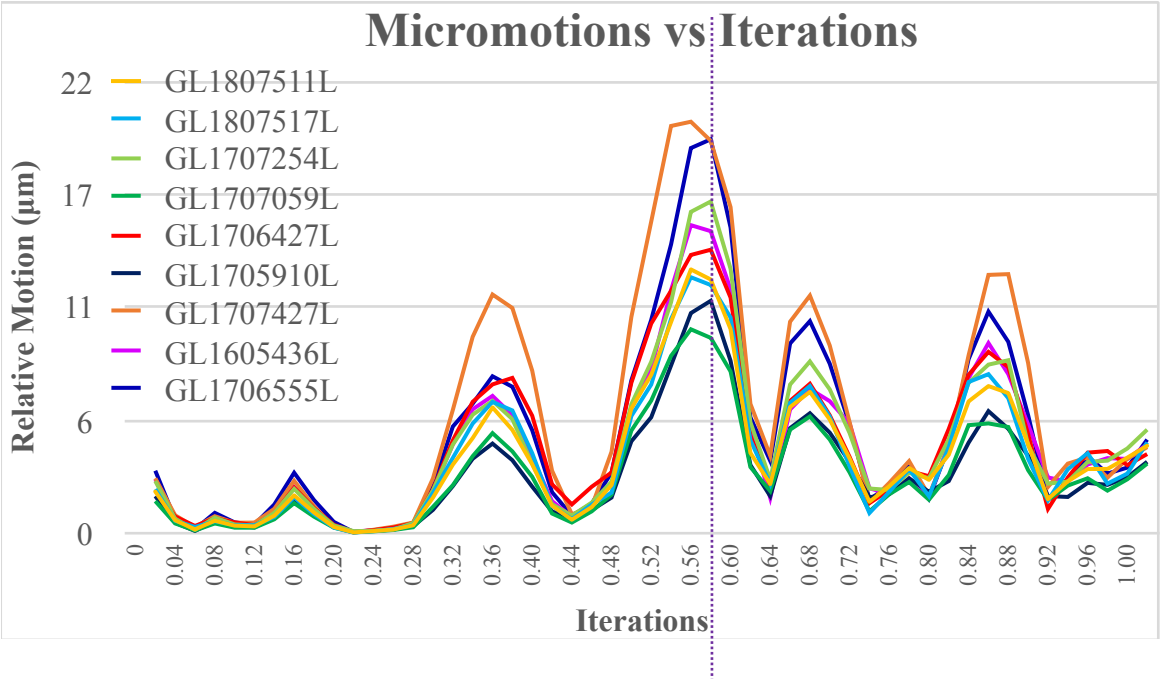

Figure 13: Micromotion vs iterations during gait of nine left tibiae

Micromotions Pattern on the Resected Surface of the Tibia

Also, using the finite element method, it is also able to visualize the micromotion and surface morphology across the entire tibial tray as demonstrated in Figure 14 (taking GL1705910L as an example here). Figure 14 showing below are the results where GL1705910L is subjected to a higher degree of the Boolean operation.

All tibial tray and the transverse view of the proximal tibia plots in this report are oriented in the same way, where the top is the anterior region, the bottom part is the posterior region, the left is the lateral region and the right is the medial region.

Figure 14 left represents the peak micromotion map across the entire tibial tray of specimen GL1705910L during gait. It is obvious that when the peak micromotion occurs, the anterior region of the tibia tray experiences more micromotion than the other regions of the tibial tray. The maximum magnitude is almost 9 μm, locating at the anterior edge of the tibial tray and micromotion tends to decrease gradually from 9 μm at the anterior edge to the center of the tibial tray. As for the posterior part of the tibial tray, it undergoes moderate micromotions of around 4 μm and micromotion also tends to decrease gradually from 4μm at the posterior edge to the center of the tibial tray. The other regions of the tibial tray are experiencing a relatively small micromotion of 1 μm or under.

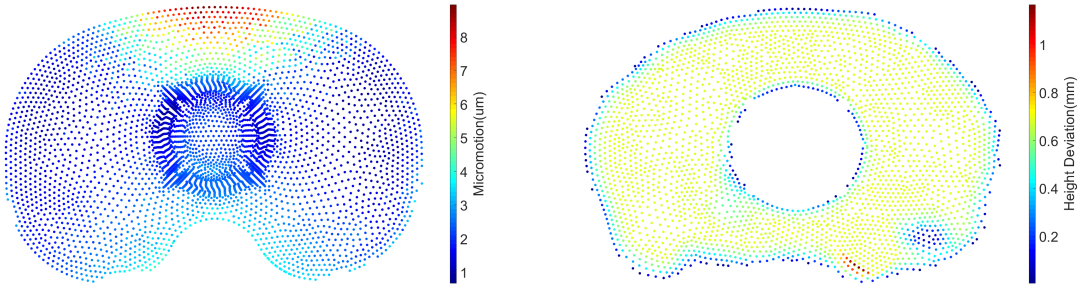

Figure 14: Peak micromotion map during gait (left) and bone surface height deviation of GL1705910L

Figure 14 right above, on the other hand, represents the surface morphology of the resected surface of the proximal tibia of specimen GL1705910L. It can be seen from the figure that the resected surface is not entirely flat. The blue part is the lower region of the entire tibia, the light green part is about 0.7 mm higher than the lowest region and the red region is about 1.1 mm higher than the lowest region.

Influence of Boolean Operation on Micromotions

Compared with a higher degree of Boolean operation which has demonstrated in above Figure 14, below Figure 15 shows a different result of GL1705910L with less degree of the Boolean operation. The peak micromotion magnitude increase from 9 µm to over 30 µm and not only that, the micromotion pattern across the entire tibial tray is different, lateral becomes the region where sees more micromotions than the rest of the tray. The micromotion also tends to decrease from over 30 µm at the lateral edge of the tray to less than 5 µm at the center of the tray. The medial edge of the tray undergoes medium micromotion of around 20 µm and the micromotion also tends to decrease as it moves to the center of the tray. Moreover, a higher magnitude of peak micromotion has been found in the rest of the models with a lower degree of Boolean operation but with a various micromotion pattern across the entire tibial tray. However, one common thing has been found that the regions where see higher micromotion tends to be at the opposite regions where the bone and the implant are in contact or in other words, where the bone surface is the highest as shown in the below Figure 15. The micromotion pattern plot and the height deviation plot of all specimens are of the same scale as shown at the right bottom edge of Figure 15.

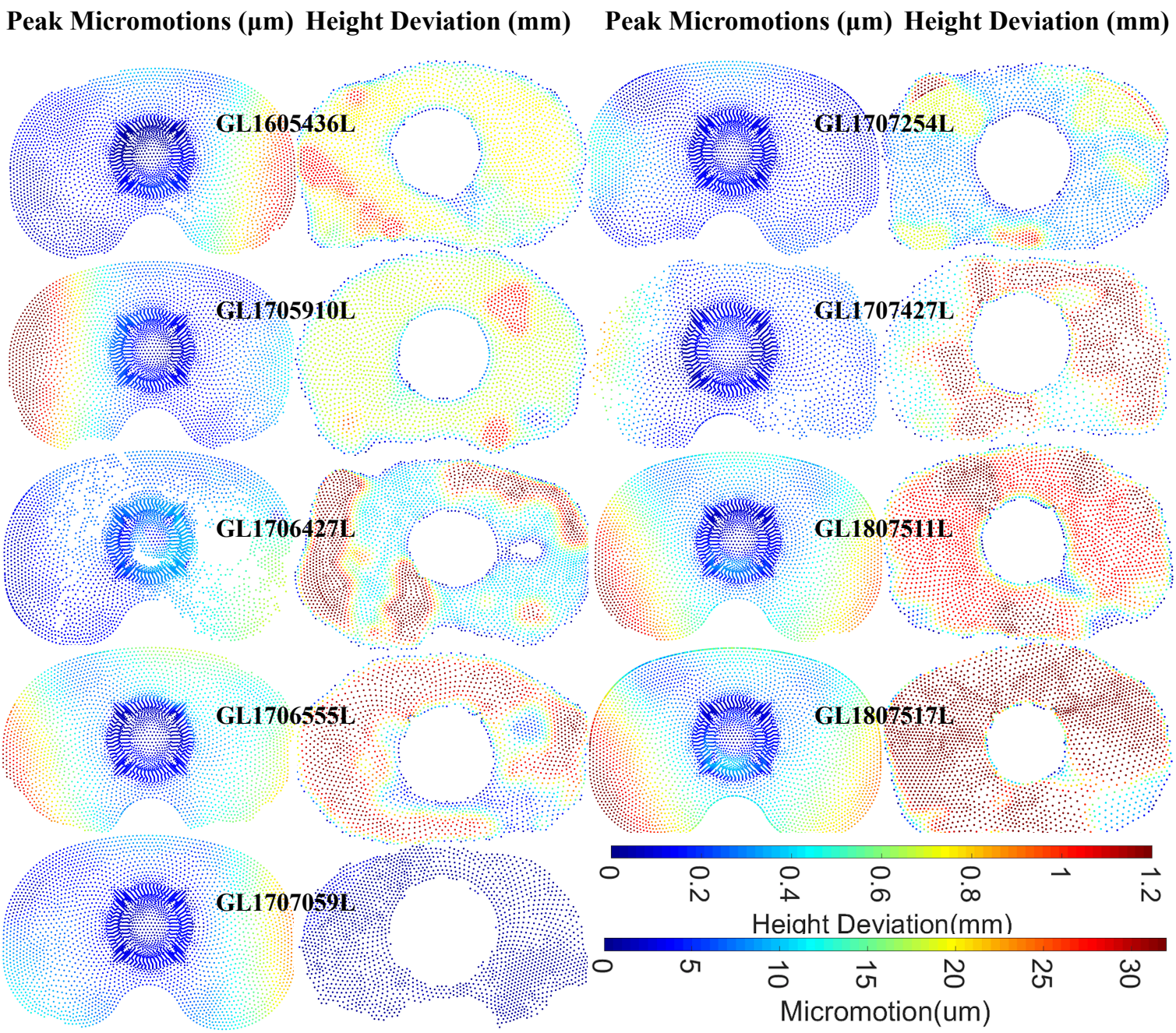

Figure 15: Peak micromotion vs surface morphology of nine left tibiae during gait

A clean-cut model has also been tested, and all models still have peak micromotion at a similar iteration range (which is from 0.56 to 0.58) and a similar micromotion vs iterations relationship as Figure 12 was found, nevertheless the tray sees a minimum peak micromotion of about 7.5 µm as demonstrated in below Figure 16. And this phenomenon does not only

appear in only one specimen, and the rest of the models with a clean-cut also results in almost identical patterns like Figure 16.

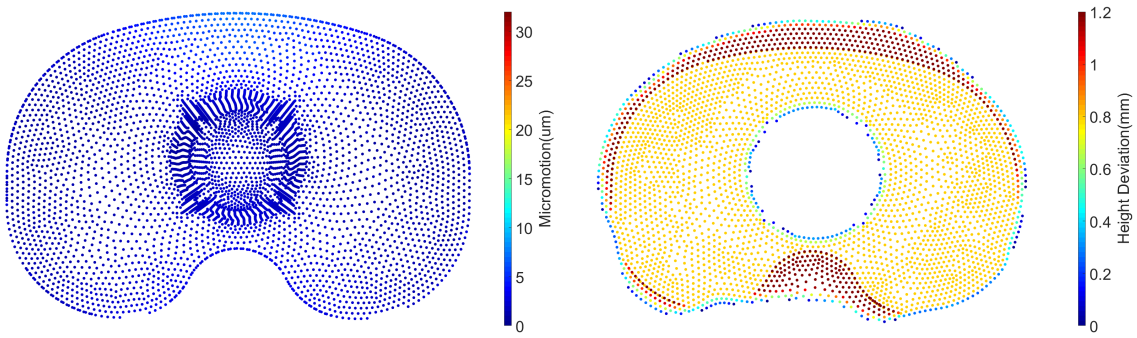

Figure 16: Peak micromotion map during gait (left) and bone surface height deviation with a clean cut of GL1705910L

Relationships between Flatness and Micromotion

As specified in the methodology part, the peak micromotion simulated via Abaqus can be concluded as below Table 4:

No.	Sample	Peak Micromotion (μm)
1	GL1605436L	34
2	GL1705910L	32.6
3	GL1706427L	41.3
4	GL1706555L	32.5
5	GL1707059L	29.4
6	GL1707254L	39.0
7	GL1707427L	30.1
8	GL1807511L	34.8
9	GL1807517L	36.6
MEAN		**34.49**
STANDARD DIVATION		**3.94**

Table 4: Peak micromotion between the proximal tibia and tibial tray

The average peak micromotion of these nine specimens during gait simulation is 34.49 µm with a 3.94 µm standard deviation (ranging from 29.4 µm to 41.3 µm). The correlations between the RMSE and the micromotion of nine left tibiae can be seen in below Figure 17.

To correlate these RMSE and peak micromotion, both the linear polynomial fit and the quadratic polynomial fit is applied as demonstrated in below Figure 17:

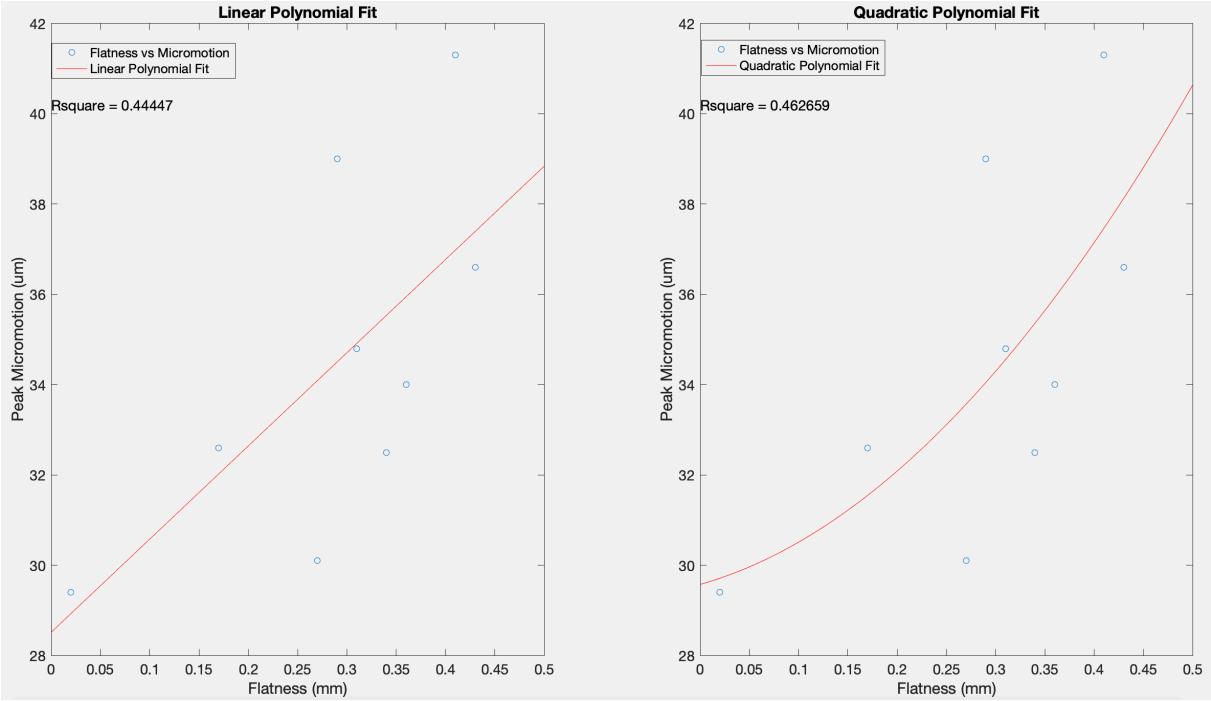

Figure 17: Peak micromotion (µm) vs RMSE (mm) of nine left tibiae during gait (left: linear polynomial fit, right: quadratic polynomial fit)

In the linear polynomial fit curve, the sum of squares due to error (SSE) is 69.005, coefficient of determination (r^2) is 0.4445 and standard error is 3.1397, while in the quadratic polynomial fit curve, SSE is 66.7462, coefficient of determination (r^2) is 0.4627 and standard error is 3.3353.

DISCUSSION

Flatness

In the results obtained in this thesis which uses the finite element method, there are similarities to the flatness quantified experimentally by earlier researchers (Toksvig-Larsen & Ryd 1991, pp. 15-8; 1994, pp. 63-6). They found that the average flatness of surgical proximal tibial cut is 0.26 mm (ranging from 0.16 mm to 0.38 mm), while this thesis finds that the average flatness of surgical proximal tibial cut is 0.29 mm with 0.13 mm standard deviation (ranging from 0.17 mm to 0.43 mm).

Micromotions Variation with Iterations

As stated in the results section and demonstrated in Figure 13, for most specimens, the peak micromotion occurs during iterations from 0.56 to 0.58. Hence, in models with a lower degree of Boolean operation, peak micromotion occurrence may have a close relationship with loading. Compared with the loading plot in Figure 7, it is evident that peak micromotion does not occur at the peak load. Instead, it occurs around 337 N axial loads acting anteriorly and posteriorly and 618 N axial loads acting medially and laterally. The occurrence is also characterized by relatively small AP direction forces acting medially and laterally, and minimal ML direction forces acting medially and laterally. Taylor, Barrett and Deffenbaugh (2012, pp. 1362-8) found that peak micromotion does not occur at the peak load, however, they found that peak micromotion occurs when there is a low axial load and a moderate VV moment, which differs from the findings of this thesis. These discrepancies may be caused by the unevenness of the surface, but further studies need to be implemented to determine this.

Based on Figure 12, there is a force or a moment causing the displacement in both the ML and AP direction. With minimal ML forces medially and laterally, the displacement in the ML direction is mainly caused by the AP force acting medially and laterally. Since the medial AP force is bigger than the lateral AP force during iterations from 0.56 to 0.58, an IE moment occurs, resulting in the displacement in the ML and AP directions. Not only are the medial AP and the lateral AP forces different in this instance, the largest difference between them occurs during these iterations, thus, the IE moment produced by AP forces medially and laterally are at the maximum. AP force medially and laterally can also cause translation in the AP

direction. This is the most likely reason why AP direction has the biggest displacement compared with the other two directions as demonstrated in Figure 12. Besides that, during this iteration, axial forces medially and laterally also have minimum discrepancy, implying a minimum VV moment.

Micromotion Pattern across the Tibial Tray

With the keel sitting in the middle of the proximal tibia, the peak micromotion is always located at the very edge of the tibial tray. The closer to the center of the tibial tray, the less micromotion is observed, regardless of the different degrees of Boolean operation in all of the models. The keel part of the tibial tray rests inside the trabecular bone of the proximal tibia, therefore it acts as the center of rotation. Moments induced by loadings will eventually rotate on an axis on which the center point is located. At the same rotational angle, the outer edge of the tray will experience more displacement than the inner part of the tray, causing a higher relative motion at the edge of the contact surface between the bone and the prosthesis.

As discussed previously, during the time frame when peak micromotion happens, the tibial tray experiences an anterior axial tension and a posterior axial compression at the same time. The equal magnitude yet opposing directions of these two forces results in a FE moment, causing the tibial tray to tilt and the anterior edge of the tibial tray to lift from the bone. This hypothesis is consistent with Figure 12 where U3 is a positive value, indicating that the bone and the tray move away from each other at the AC location of the tibial tray due to the AP axial forces. At that moment, the compression of ML axial forces acts in the same direction and almost with the same magnitude, therefore it does not result in an effective or significant VV moment. This explains the lack of micromotion at the medial or lateral regions of the tibial tray.

The micromotion pattern found in this study is also quite different from the findings of previous studies. Even in a clean-cut model, the peak micromotion usually occurs at the AC edge of the tibial tray, which is different from what was reported by Taylor, Barrett and Deffenbaugh (2012, pp. 1362-8). Their study found that the peak micromotion is located at the lateral edge of the LCS tibial tray. These discrepancies could lie in different loading, but further studies need to be conducted to verify this.

Influence of Boolean Operation on Micromotions

As mentioned in the influence of Boolean operation on micromotions in results, the more the bone was cut, the less effect will the flatness has on the micromotion. The degree of Boolean operation does not only affects the micromotion magnitude, but also the micromotion pattern across the entire tibial tray. For instance, a clean-cut sees a minimum peak micromotion and vice versa. Contrary to what we find in the models with a lower degree of Boolean operation, loading as a variable plays a more dominant role in the micromotion pattern across the tray in this situation. However, in a lower degree of Boolean operation model, as demonstrated in Figure 15 above, it presents a completely different micromotion pattern across the entire tibial tray as well as a higher magnitude of peak micromotion. The highest regions of the bone resected surface act as a fulcrum of the entire tray, resulting in the tilting effect of the tibial tray. Consequently, the micromotion patterns of these models are highly dependent on the surface morphology of the resected proximal tibia.

The micromotion pattern across the tibial tray or the magnitude of the peak micromotion do not only lie in the degrees of Boolean operation, but they are also closely correlated with the matrix transformation, especially in the implanted proximal tibia with a lower degree of the Boolean operation. How the resected surfaces of the proximal tibia appear in the final models can vary with various rotated angle previous in Simpleware, causing different magnitudes of the peak micromotion as well as the micromotion pattern across the entire tibial tray. It was also mentioned that, apart from the micromotion magnitude, the overall fashion of micromotion vs iterations plot does not change much of its shape, indicating that the degree of Boolean operation might have a bigger impact on the magnitude of micromotion but a smaller effect when the peak micromotion happens.

Relationships between Flatness and Micromotion

The peak micromotion found in these models with a lower degree of Boolean operation is 34.49 μm (ranging from 29.4 μm to 41.3 μm) with a standard deviation of 3.94 μm, which is lower than the study done by Taylor, Barrett and Deffenbaugh (2012, pp. 1362-8). They have obtained a mean peak micromotion ranging from 92 μm to 106 μm for LCS. There is a

possibility that the Young's modulus assigned in this thesis for the proximal tibia (as demonstrated in Figure 5) is higher than the normal value. This might be due to the methodology used to calibrate the greyscale data is not good enough to achieve an accurate greyscale map of the bone, and the method tends to over predict the Hounsfield unit of the bone marrow.

From the results plotted in above Figure 17, moderate correlated polynomial relationships are found between flatness and peak micromotion with a coefficient of determination of over 0.45. Generally, the higher is the RMSE, the higher the peak micromotion will be. However, there exists some inaccuracies or individual discrepancies. For instance, specimens GL1705910L, GL1707059L, and GL1807517L fall a bit far from the RMSE trend. The relationships found are not highly correlated with a moderate R squared. It is recommended that a larger sample group and a more accurate quantification method could be applied to further investigate the relationships between the flatness and the micromotion. There are a few reasons for the inaccuracies in the quantification of the flatness and the peak micromotion in the methodology applied in this study. Firstly, the transformation of the matrix or the 3D image rotation issues could be the leading factors that cause these inaccuracies.

Finding vectors in each plane and trying to align the three vectors with the global coordinate x, y and z-axis respectively could involve some subjective factors, leading to different values of RMSE. Apart from that, since the top resected surface nodes are selected using a range of z vertices from the maximum to few millimeters away from it. By choosing different vertical tolerances will also result in different RMSE. Lastly, the nodes selected to quantify the flatness do not only lie beneath the tibial tray but also around them. As a result, the nodes that are slightly away from the tray and not involved in the contact mechanism are also selected to obtain RMSE. Therefore, the method used to select the nodes may also contribute to errors in the results.

Further Investigation

Experimental validation of the model

To be able to validate the finite element model, there are some gaps between the experimental model and the computational model need to be narrowed. Firstly, the nodes selected to calculate the micromotion in the finite element model need to be as close as possible to the

experimental model. In this study, the nodes selected in this finite element model mostly are based on the experimental model which are respectively located at AC, AL and AM at the edge of the tibial tray and vertically 5mm underneath them on the outer surface of the proximal tibia due to the difficulties of fixing the displacement sensors at the interface experimentally. Therefore, there will be some errors in calculating micromotions, which are mainly induced by elastic deformations of both the bone and the tibial tray. Secondly, the nodes that the loadings applied to need to be as close as possible to the experimental model too. In this study, the nodes selected are respectively located anteriorly, posteriorly, laterally and medially and each force is distributed into 10 nodes in each region. Moreover, due to the lack of patients' file, a modified loading data scaled to the body weight of individual patients has not been conducted yet, but, to be able to validate this finite element model, a scaled loading file is essential. Finally, multicyclic loading could be applied instead of only one cycle since the unevenness of the resected surface might undergo a subtle change and the simulated displacement might become more stable after one or two cycles. Due to the limitation of time, multicycle loading has not been implemented in all models in this study and therefore the results are not presented here.

A more comprehensive comparison

Further studies need to be conducted on whether bone-prosthesis contact surface morphology or loading has a more dominant effect on the micromotion pattern or the magnitude of the peak micromotion. Due to the limitation of time in this study, a more comprehensive comparison with the clean-cut and the uneven tibial resected surface has not been conducted. Also, since level gait is the most common activity and can cause representative peak micromotions, other daily activities like stair ascent, stair descent, squat or deep knee bending have not been simulated in this study, but it is an important perspective to carry on in further studies. Furthermore, this study only demonstrates the micromotion pattern across the entire tibial tray at the incident of peak micromotion since peak micromotion is the most important factor that could cause failure of osteointegration in a cementless fixation knee replacement and we want to investigate the worst-case scenario, but other time frames are also required to be further looked into to have a deeper understanding of the influence of flatness on micromotion. Finally, in this thesis, only representative nodes are selected to obtain the

relationships between micromotion and iterations. To be specific, the nodes selected are mainly at three locations namely the anterior center (AC) edge of the tray, the anterior lateral (AL) edge of the tray, and the anterior medial (AM) edge of the tray. This will probably be enough with a higher degree of Boolean operation since the peak micromotion is usually located at the AC edge of the tibial tray. However, in some models with a lower degree of Boolean operation, the peak micromotion often occurs at the edge of the tibial tray medially or laterally, or even slightly off to the posterior area as shown in Figure 15. Thus, a more comprehensive surface node needs to be further discovered to compare in terms of the changes of micromotion with iterations.

A more physiological loading

The loading simplification in this thesis refers a previous study done by Fitzpatrick, Hemelaar and Taylor (2014, pp. 1718-26), but it has limitations when representing the physiological loading condition during activities. As an illustration, the FE moment, generated from the axial forces acting anteriorly and posteriorly in this thesis, should be generated from the forces from the patellar tendon and hamstring muscle attached to the tibia in reality. This may be an important factor affecting the micromotion between the tibia and the implant. Thus, further study on how the simplification of the loading will influence the micromotion need be investigated.

Optimizations

Material property / Bone quality

As discussed in the relationship between flatness and micromotion, the peak micromotion found in this study is lower than other studies. The reason could lie in the material property assigned previously in this study. This leads to the question whether bone quality like bone apparent density or material property like Young's modulus will potentially correlate with the micromotion too. Hence, further studies will need to be conducted to determine their relationships with micromotion respectively.

Press fit or impaction

In this study, the effects of press-fit or impaction have not been taken into considerations. However, they are crucial factors when it comes to cementless fixation, because in the

surgery, press-fit or impaction is usually involved in a cementless fixation. Therefore, inevitably, the experimental validation of the study will include some degree of impaction, which might differ from what is set up in this study.

Convergence study

The mesh size used in this study coincides with that used in previous study (Awadalla et al. 2018, pp.1876-86), but due to the different outcomes between the two studies, a convergence study is recommended. The reason to carry out the convergence study is to determine a more appropriate model mesh size to better converge with the experimental results. To save the computational cost and obtain a maximum outcome, perhaps only a finer mesh at the contact interface could be taken into consideration.

CONCLUSION

To conclude what has been found in this study: Firstly, a moderate polynomial relationship is found between the flatness of the tibia and peak micromotion with a coefficient of determination of more than 0.45. Furthermore, peak micromotion does not occur at the peak axial load of the entire cycle. Instead, it occurs at minimal ML direction loads, at low AP direction loads, and at moderate axial loads. The occurrence is also characterized by low FE moments, maximal IE moments, and minimal VV moments. The degree of Boolean operation has a large effect only on the magnitude of peak micromotion, and has little effect on the instance when peak micromotion occurs. This implies that it is highly likely that loadings have a more dominant effect on the instance when peak micromotion occurs compared with surface morphology. Lastly, the FE moment produced by a moderate anterior axial tension and a posterior axial compression lifts the tray anteriorly. Although the surface morphology of the resected surface has a subtle effect on the instance when peak micromotion occurs, it has a large effect on the micromotion pattern across the entire tibial tray. Apart from that, the magnitude of the micromotion also tends to increase with an increase in the unevenness of the surgical cut. This indicates that compared with loadings, surface morphology is likely to have a more dominant effect on micromotion pattern and magnitude in an uneven surface.

This study may be a pioneer of its kind in bringing a significant factor, the flatness of surgical cut, into the finite element model of bone implantation. Implant design may thus be further optimized and improved. Nevertheless, more accurate methods and optimization are necessary to further investigate the relationship between the flatness of the surgical cut and micromotion between the implant and the bone.

REFERENCES

1. Aebli, N, Krebs, J, Schwenke, D, Hii, T & Wehrli, U 2004, 'Progression of Radiolucent Lines in Cementless Twin-Bearing Low-Contact-Stress Knee Prostheses - A Retrospective Study', The Journal of Arthroplasty, Vol. 19, pp.783-9.

2. Australian Bureau of Statistics (ABS), National Health Survey (NHS) 2014-2015, ABS cat. no. 4324.0.55.001, Australian Bureau of Statistics, Canberra.

3. Australian Orthopaedic Association National Joint Replacement Registry (AOANJRR) 2018, 'Hip, Knee & Shoulder Arthroplasty: 2018 Annual Report', Adelaide: AOA, 2018.

4. Awadalla, M, Al-Dirini, RMA, O'Rourke, D, Solomon, LB, Heldreth, M & Taylor, M, 'Influence of Varying Stem and Metaphyseal Sleeve Size on the Primary Stability of Cementless Revision Tibial Trays Used to Reconstruct AORI IIA Defects. A Simulation Study', The Journal of Orthopaedic Research, Vol. 36, pp. 1876-86.

5. Barker, DS, Tanner, KE & Ryd, L 2005, 'A circumferentially flanged tibial tray minimizes bone-tray shear micromotion', Proceedings of the Institution of Mechanical Engineers, Part H: The Journal of Engineering in Medicine, Vol. 219, pp. 449-56.

6. Baker, PN, Khaw, FM, Kirk, LMG, Esler, CNA & Gregg, PJ 2007, 'A randomised controlled trial of cemented versus cementless press-fit condylar total knee replacement', The Journal of Bone and Joint Surgery, Vol. 89-B, pp. 1608-14.

7. Bryan, R, Mohan, PS, Hopkins, A, Galloway, F, Taylor, M & Nair, PB 2010, 'Statistical modelling of the whole human femur incorporating geometric and material properties', Medical Engineering & Physics, Vol. 32, pp.57–65.

8. Carlsson, L, Rostlund, T, Albrektsson, B & Albrektsson, T 1988, 'Implant fixation improved by close fit. Cylindrical implant-bone interface studied in rabbits', Acta Orthopaedica Scandinavica, Vol. 59, pp. 272-5.

9. Carter DR & Hayes WC 1997, 'The compressive behavior of bone as a two-phase porous structure', The Journal of Bone and Joint Surgery, Vol. 59, pp. 954–62.

10. Chong, DY, Hansen, UN & Amis, AA 2010, 'Analysis of bone-prosthesis interface micromotion for cementless tibial prosthesis fixation and the influence of loading conditions.', The Journal of Biomechanics, Vol. 43, pp. 1074-80.

11. Chong, DY, Hansen, UN, van der Venne R, Verdonschot, N & Amis, AA 2011, 'The influence of tibial component fixation techniques on resorption of supporting bone stock after total knee replacement', The Journal of Biomechanics, Vol. 44, pp. 948-54.

12. Costi, J 2017, 'Cartilage', lecture notes distributed in the topic ENGR8732 Biomechanics GE, Flinders University, Tonsley, August.

13. Costi, J 2017, 'Ligament and Tendon', lecture notes distributed in the topic ENGR8732 Biomechanics GE, Flinders University, Tonsley, August.

14. Dassault Systèmes 2010, Abaqus Analysis user's Manual, Abaqus 6.10 Online Documentation, viewed 27 May, <https://www.sharcnet.ca/Software/Abaqus610/Documentation/docs/v6.10/books/usb/default.htm?startat=pt09ch32s03aus137.html>.

15. Fitzpatrick, CK, Baldwin, MA, Clary, CW, Maletsky, LP & Rullkoetter, PJ 2014, 'Evaluating knee replacement mechanics during ADL with PID-controlled dynamic finite element analysis', Computer Methods in Biomechanics and Biomedical Engineering, vol. 17, pp. 360-9.

16. Fitzpatrick, CK, Hemelaar, P & Taylor, M 2014, 'Computationally efficient prediction of bone-implant interface micromotion of a cementless tibial tray during gait', The Journal of Biomechanics, Vol. 47, pp. 1718-26.

17. Galloway, F, Kahnt, M, Ramm, H, Worsley, P, Zachow, S, Nair, P & Taylor, M 2013, 'A large scale finite element study of a cementless osseointegrated tibial tray', The Journal of Biomechanics, Vol. 46, pp. 1900-6.

18. GBD 2017 Disease and Injury Incidence and Prevalence Collaborators, 'Global, regional, and national incidence, prevalence, and years lived with disability for 354 diseases and injuries for 195 countries and territories, 1990–2017: a systematic analysis for the Global Burden of Disease Study 2017', Lancet, Vol. 392, pp. 1789-858.

19. Ghosh, R, Pal, B, Ghosh, D & Gupta, S 2015, 'Finite element analysis of a hemi-pelvis: the effect of inclusion of cartilage layer on acetabular stresses and strain', Computer Methods in Biomechanics and Biomedical Engineering, Vol. 18 pp. 697–710.

20. Glyn-Jones, S, Palmer, AJ, Agricola, R, Price, AJ, Vincent, TL, Weinans, H & Carr AJ 2015, 'Osteoarthritis', Lancet, Vol. 386, pp. 376-87.

21. Gill, TJ, Van de Velde, SK, Wing, DW, Oh, LS, Hosseini, A & Li, G 2009, 'Tibiofemoral and Patellofemoral Kinematics After Reconstruction of an Isolated Posterior Cruciate Ligament Injury: In Vivo Analysis During Lunge', The American Journal of Sports Medicine, Vol. 37, pp. 2377-85.

22. Hashemi, A, Shirazi-Adl, A & Dammak, M 1996, 'Bidirectional Friction Study of Cancellous Bone-Porous Coated Metal Interface', The Journal of Biomedical Material Research, Vol. 33, pp. 257-67.

23. Helgason, B, Perilli, E, Schileo, E, Taddei, F, Brynjolfsson, S & Viceconti, M 2008, 'Mathematical relationships between bone density and mechanical properties: A literature review', Clinical Biomechanics, Vol. 23, pp. 135-46.

24. Keja, M, Wevers, HW, Siu, D & Grootenboer, H 1994, 'Relative motion at the bone-prosthesis interface', Clinical Biomechanics, Vol. 9, pp. 275-83.

25. Kraemer, WJ, Harrington, IJ & Hearn, TC 1995, 'Micromotion secondary to axial, torsional, and shear loads in two models of cementless tibial components', The Journal of Arthroplasty, Vol. 10, pp. 227-235.

26. Kulowski, J 1932, 'Flexion contracture of the knee: The mechanics of the muscular contracture and the turnbuckle cast method of treatment: with a review of fifty-five cases', The Journal of Bone and Joint Surgery, Vol. 14, pp. 618–63.

27. Kutzner, I, Heinlein, B, Graichen, F, Bender, A, Rohlmann, A, Halder, A, Beier, A & Bergmann, G 2010, 'Loading of the knee joint during activities of daily living measured in vivo in five subjects', The Journal of Biomechanics, Vol. 43, pp. 2164-73.

28. Lombardi, AVJ, Berasi, CC & Berend, KR 2007, 'Evolution of Tibial Fixation in Total Knee Arthroplasty', The Journal of Arthroplasty', Vol. 22, pp. 25-9.

29. Masouros, SD, Bull, AMJ & Amis, AA 2010, 'Biomechanics of the knee joint', Orthopaedics and Trauma, Vol. 24, pp. 84-91.

30. Matthews, LS & Goldstein, SA 1986, 'Caused and prevention - (i) Biomechanics', Current Orthopaedics, Vol. 1 pp. 27-33.

31. Morgan, EF, Bayraktar, HH & Keaveny, TM 2003, 'Trabecular bone modulus–density relationships depend on anatomic site', The Journal of Biomechanics, Vol. 36, pp. 897–904.

32. Mow, VC, & Huiskes, R 2004, Basic orthopaedic biomechanics and mechano-biology, 3rd edn, Wolters Kluwer Health, Philadelphia, USA.

33. National Institute of Arthritis and Musculoskeletal and Skin Diseases 2016, 'Osteoarthritis', National Institute of Health, viewed 3 March 2019, <https://www.niams.nih.gov/health-topics/osteoarthritis>.

34. Navacchia, A, Clary, CW, Wilson, HL, Behnam, YA & Rullkoetter, PJ 2018, 'Validation of model-predicted tibial tray-synthetic bone relative motion in cementless total knee replacement during activities of daily living', The Journal of Biomechanics, Vol. 77, pp. 115-23.

35. Nissan, M 1980, 'Review of some basic assumptions in knee biomechanics', The Journal of Biomechanics, vol. 13, pp: 375-81.

36. Palmer, S & Cross, M n.d., 'Total knee replacement', North Sydney Orthopaedics and Sports Medicine Centre and Australian Institute of Musculoskeletal Research, viewed 27 May 2019, <http://www.kneeclinic.com.au/papers/TKR/tkrchapter.htm>.

37. Perillo-Marcone, A, Ryd, L, Johnsson, K & Taylor, M 2004, 'A combined RSA and FE study of the implanted proximal tibia: correlation of the post-operative mechanical environment with implant migration', The Journal of Biomechanics, Vol. 37, pp. 1205-13.

38. Pilliar, RM, Lee, JM & Maniatopoulos, C 1986, 'Observations on the effect of movement on bone ingrowth into porous-surfaced implants', Clinical Orthopaedics and Related Research, Vol. 208, pp. 108-13.

39. Platzer, W 2004, Color Atlas and Textbook of Human Anatomy, Vol. 1. Locomotor System, Thieme Publishing Group, Stuttgart.

40. Sala, M, Taylor, M & Tanner, KE 1999, 'Torsional stability of primary total knee replacement tibial prostheses: a biomechanical study in cadaveric bone', The Journal of Arthroplasty, Vol. 14, pp. 610-5.

41. Sandbom, PM, Cook, SD, Anderson, RC, Spires, WP & Kester, MA 1987, 'The effect of surgical fit on hone growth into porous coated implants', Trans 33rd Annual Meeting Orthopaedics Research Society, pp. 217.

42. Sorrells, RB 2014, LCS Complete Milestone Surgical Technique, DePuy Synthes Joint Reconstruction, Warsaw, IN, US.

43. Synopsys, Inc. 2016, Tutorial Guide, Synopsys, Inc., San Jose, US.

44. Taylor, M, Barrett, DS & Deffenbaugh, D 2012, 'Influence of Loading and Activity on the Primary Stability of Cementless Tibial Trays', The Journal of Orthopaedic Research, Vol. 30, pp. 1362-8.

45. Taylor, M, Deffenbaugh, D & Heldreth, M 2010, 'Influence of alignment on the primary stability of cementless tibial trays: a combined KneeSim and finite element study', Poster No. 2114, 56th Annual Meeting of the Orthopaedic Research Society.

46. Taylor, M, Tanner, KE & Freeman, MA 1998, 'Finite element analysis of the implanted proximal tibia: a relationship between the initial cancellous bone stresses and implant migration', The Journal of Biomechanics, Vol. 31, pp. 303-10.

47. The International Organization for Standardization 2011, Geometrical product specifications (GPS) — Flatness — Part 1: Vocabulary and parameters of flatness , ISO 12781-1, International Standard, Switzerland.

48. Tissakht, M, Eskandari, H & Ahmed, AM 1995, 'Micromotion analysis of the fixation of total knee tibial component', Computers & Structures, Vol. 56, pp. 365-75.

49. Toksvig-Larsen, S & Ryd, L 1991 'Surface flatness after bone cutting: A cadaver study of tibial condyles', Acta Orthopaedica Scandinavica, Vol. 62, pp. 15-8.

50. Toksvig-Larsen, S & Ryd, L 1994 ‘Surface Characteristics Following Tibial Preparation During Total Knee Arthioplasty’, The Journal of Arthroplasty, Vol. 9, pp. 63-6.

51. Walker, PS, Hsu, HP & Zimmerman, RA 1990, ’A comparative study of uncemented tibial components’, The Journal of Arthroplasty, Vol. 5, pp. 245-53.

52. Wikipedia: the free encyclopaedia 2019, ‘Knee’, Wikimedia Foundation Inc., viewed 25 February 2019, <https://en.wikipedia.org/wiki/Altmetrics>.